Available online at www.sciencedirect.com
ScienceDirect
Trans. Nonferrous Met. Soc. China 26(2016) 2857−2867
Transactions of Nonferrous Metals Society of China
www.tnmsc.cn

Effect of flow velocity on corrosion behavior of AZ91D magnesium alloy at elbow of loop system

Jing TIAN[1], Hua-liang HUANG[1,2], Zhi-quan PAN[1], Hong ZHOU[1]

1. School of Chemistry and Environmental Engineering, Wuhan Institute of Technology, Wuhan 430073, China;
2. School of Chemistry and Chemical Engineering,
Huazhong University of Science and Technology, Wuhan 430074, China

Received 27 October 2015; accepted 10 May 2016

Abstract: A loop system was used to investigate the effect of flow velocity on corrosion behavior of AZ91D magnesium alloy at an elbow of loop system based on array electrode technology by polarization, computational fluid dynamics (CFD) simulation and surface analysis. The experimental results showed that the corrosion rate increased with increasing flow velocity, and a critical flow velocity could exist in the corrosion of AZ91D magnesium alloy. When flow velocity exceeded the critical flow velocity, fluid hydrodynamics was dominant in the corrosion of AZ91D magnesium alloy. On the contrary, the electrochemical factors were dominant.

Key words: magnesium alloy; flow velocity; elbow; computational fluid dynamics (CFD); polarization

1 Introduction

Corrosion, especially flow-assisted corrosion (FAC), is one of the main reasons resulting in failure of the heat exchanger in cooling system [1−4]. Magnesium alloys are regarded to be promising alternatives to aluminum alloys and steel used in the automotive industry because of their light density, high specific strength and good mechanical properties [5,6], especially in the cooling system of an engine block. However, the corrosion of magnesium alloys is a major problem and restricts their applications in the cooling system of the engine block [7]. During the past decade, many research works have been focused on corrosion behavior and mechanism of magnesium alloys [8−14].

AZ91D magnesium alloy is one of the most popular magnesium alloys, which is used in the automotive industry, and many works have been done to investigate its corrosion behavior and mechanism in a static state solution [12−14], but the corrosion behavior and mechanism of AZ91D magnesium alloy are not reported in a flowing medium so far. Because the flow-condition has important effects on the mass transfer process and the removal of corrosion products on the electrode surface [15−17], different corrosion behaviors of AZ91D magnesium alloy are expected in a flowing medium.

FAC has been studied using rotating disk electrode (RDE) or rotating cylinder electrode (RCE) [18−20], impingement jet system [21−23] and loop system [15,24,25]. However, RDE, RCE and impingement jet system could not really reflect the flow pattern in a pipe. Therefore, a loop system should be applied to simulating the realistic flow environment in a pipe.

Elbow is an important part in the heat exchanger configuration. However, the flow pattern will generate great changes in flow direction and flow velocity in a 90° elbow, resulting in significant difference in the corrosion behavior at different locations of the elbow [26]. The wall thinning is exacerbated at the elbow by FAC due to the sudden change in the flow pattern. Therefore, FAC at the elbow is rather serious among the damages of the heat exchanger. Apparently, there should be correlation between the corrosion behavior at different locations of the elbow and the flow pattern. However, there is little study on the corrosion behaviors at different locations of the elbow [15]. Array electrode technique could be used for studying the corrosion behaviors at different locations

Foundation item: Project (51401151) supported by the National Natural Science Foundation of China; Projects (2015T80792, 2012M511207) supported by the Postdoctoral Science Foundation of China
Corresponding author: Hua-liang HUANG; Tel: +86-27-87543432; Fax: +86-27-87543632; E-mail: hhl0425@aliyun.com
DOI: 10.1016/S1003-6326(16)64414-X

of the elbow.

In this work, a loop system was used to study the effect of flow velocity on corrosion behavior of AZ91D magnesium alloy at a 90° elbow in circulating ASTM D1384−87 solution based on array electrode technology by polarization, computational fluid dynamics (CFD) simulation and surface analysis. The corrosion behaviors at different locations of the elbow with different flow velocities were also investigated to determine the fluid hydrodynamics effects at a 90° elbow. The corrosion mechanism of AZ91D magnesium alloy under different flow velocities was discussed.

2 Experimental

2.1 Loop system for corrosion test

Figure 1(a) shows the circulating loop system used for corrosion test. It was made up of pipes, a centrifugal pump, a container, a pressure gage, a flow meter and array electrode test section. The solution was supplied from a 125L container and circulated through the centrifugal pump. The flow velocity was controlled by controlling the pump rotational speed using a controller. The flow velocities in this study are 1.77, 3.54 and 5.31 m/s which were measured by using the flow meter, respectively. The loop system was made of 316L stainless steel pipe with an inner diameter of 50 mm. After pretreatment, these array electrodes were mounted into the elbow test section with the same spacing distance in flow direction. Figure 1(b) shows the schematic diagram of the test section. Figure 1(c) shows the photograph of the test section with 20 specimens at the elbow. The exposed surfaces of these array electrodes were in accordance with the internal surface of pipe, as shown Fig. 1(d). 20 specimens at the elbow are symmetrical with respect to the central plane of pipe. In addition, a specimen (No. 1 electrode) is in the straight pipe after the outlet of the elbow, the other specimen (No. 7 electrode) is in the straight pipe before the inlet of the elbow.

2.2 Electrode and solutions

These array electrodes were made up of AZ91D magnesium alloy with identical diameter of 5 mm and height of 60 mm. The specimens were embedded in epoxy resin, leaving a working area of 19.625 mm^2. The working surface was polished with 1200 grit emery papers, and then cleaned by distilled water and pure ethanol.

The test solution was ASTM D1384−87 solution (pH=8.2) containing 148 mg/L (1.04 mmol/L) Na_2SO_4 + 138 mg/L (1.64 mmol/L) $NaHCO_3$ + 165 mg/L (2.82 mmol/L) NaCl, which was made up from analytical grade reagents and deionized water.

2.3 Polarization measurements

An electrochemical test system CS350 (Wuhan Corrtest Instruments Corp., Ltd., Wuhan, China) was used for polarization curve measurement during corrosion test. A three-electrode electrochemical cell was

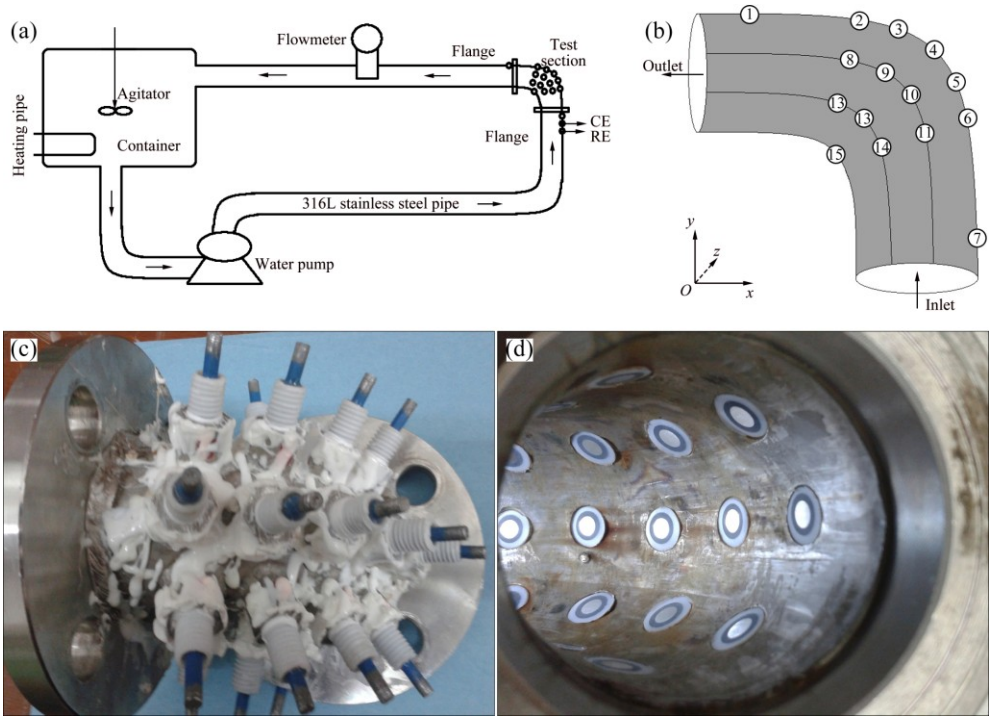

Fig. 1 Schematic diagrams of corrosion loop test system and array electrodes: (a) Loop test system; (b) Distribution of array electrodes in test section; (c) Assembly of elbow test section; (d) Distribution of array electrodes at inner wall of elbow

constructed with single AZ91D magnesium alloy electrode as working electrodes (WE), a platinum plate as counter electrode (CE) and a saturated calomel electrode (SCE) as reference electrode (RE), CE and RE were located in the straight pipe before the inlet of the elbow and closer to these array electrodes, as shown Fig. 1(a). Polarization curve was measured on single AZ91D magnesium alloy electrode at a potential sweep rate of 1 mV/s. The test was performed with different flow velocities at room temperature (about 25 °C) and an atmospheric pressure.

2.4 Surface morphology analysis after corrosion test

After corrosion for 4 h, surface morphologies of AZ91D magnesium alloy electrodes were observed by an optical microscope (VHX−1000E, Keyence, Japan).

2.5 CFD simulation

Professional fluid simulation software fluent was employed to perform CFD simulation. Pre-processing software Gambit was used to establish the geometric model. The straight section before the inlet of elbow was set as 0.5 m and the straight section after the outlet of elbow was also set as 0.5 m. Volume meshes were constructed with the interval size of 0.01 m. The different flow velocities (1.77, 3.54 and 5.31 m/s, respectively) at the inlet and an atmospheric pressure (101.325 kPa) at the outlet were set as the boundary conditions. The fluid was assumed to be incompressible and a k−ε turbulent model (double equation model, k is turbulent kinetic energy and ε is kinetic energy dissipation rate) was used to numerically solve the simulation since the fluid flowed at Reynolds numbers of 88500, 177000 and 265500 (calculated according to the inner diameter of pipe and different flow velocities). The Reynolds numbers were much greater than 4000, indicating a turbulent flow. Turbulence intensity (calculated according to the calculated Reynolds number and I=0.16$Re^{-1/8}$) in the simulation was 3.36%, 3.53% and 3.85%, respectively. The k−ε turbulence equation was solved by iterative method with a convergence criterion of 0.00001.

3 Results

3.1 Polarization curve measurements

Polarization curves of AZ91D magnesium alloy array electrodes under static state condition and different flow velocities (μ) are shown in Figs. 2−5. It is seen from Figs. 2−5 that these electrodes are in an active dissolution state under different flow conditions, and these polarization curves of all the specimens exhibit the same shape. The polarization curves can be analyzed through cathodic Tafel extrapolation [27]. The

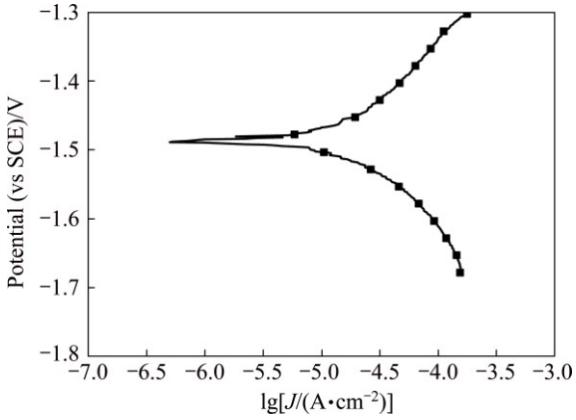

Fig. 2 Polarization curves of array electrodes under static state condition

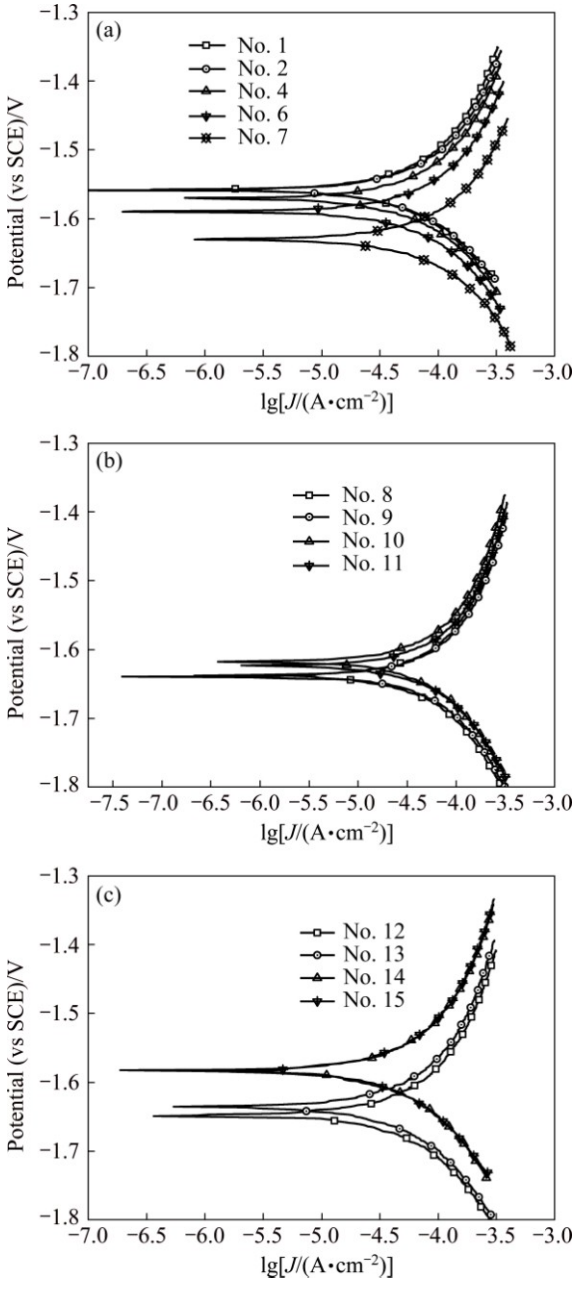

Fig. 3 Polarization curves of array electrodes under flow velocity of 1.77 m/s

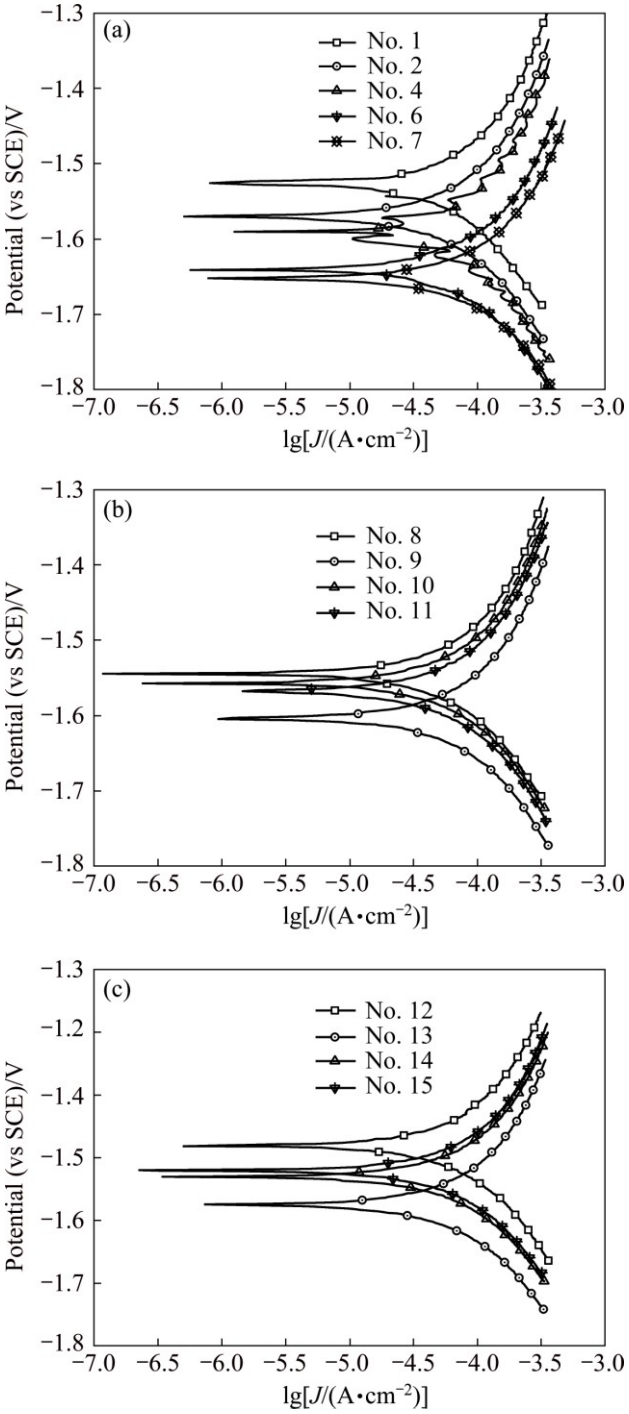

Fig. 4 Polarization curves of array electrodes under flow velocity of 3.54 m/s

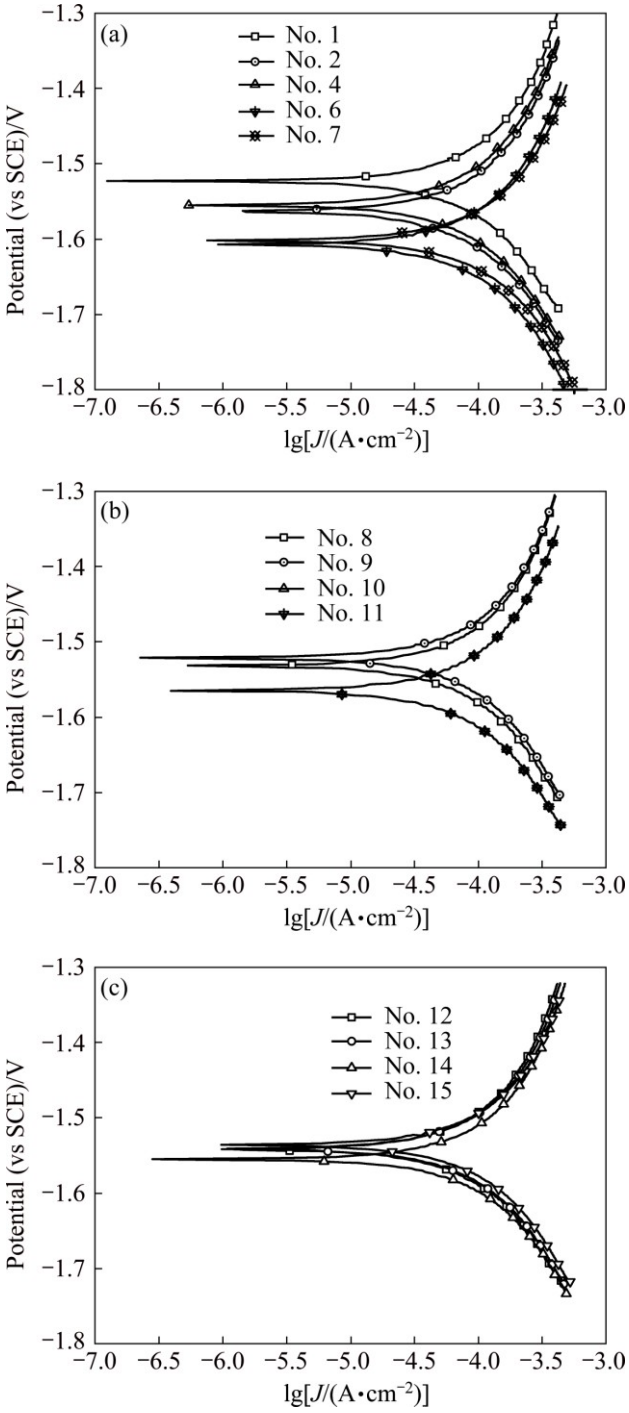

Fig. 5 Polarization curves of array electrodes under flow velocity of 5.31 m/s

electrochemical parameters, including corrosion potential (φ_{corr}), corrosion current density (J_{corr}) and cathodic Tafel slope (b_c) are fitted and listed in Tables 1−4. The corrosion current density increases with increasing flow velocity. When the flow velocity is 5.31 m/s, the corrosion current density increases from the outer wall to the inner wall and the minimum corrosion current density appears at the outermost side at the elbow. However, when flow velocity is 1.77 m/s, the corrosion current density decreases from the outer wall to the inner wall and the minimum corrosion current density appears at the innermost side at the elbow. When the flow velocity is 3.54 m/s, the minimum corrosion current density appears between the outer wall and the inner wall at the elbow (No. 12 electrode). The corrosion rate for No. 7 electrode is the highest among all of these electrodes under different flow velocities, which could be attributed to the minimum solution resistance due to the nearest distance from CE (Fig. 1(a)).

Table 1 Fitting parameters of polarization curves of AZ91D magnesium alloy under static state condition

φ_{corr}(vs SCE)/ mV	b_c (vs SCE)/ (mV·dec^{-1})	Corrosion current density/(A·cm^{-2})
−1489	−205.2	2.53×10^{-5}

Table 2 Fitting parameters of polarization curves of array electrodes under flow velocity of 1.77 m/s

Electrode No.	φ_{corr} (vs SCE)/ mV	b_c (vs SCE)/ (mV·dec^{-1})	Corrosion current density/(A·cm^{-2})
1	−1610	−218.1	5.76×10^{-5}
2	−1611	−225.6	6.37×10^{-5}
3	−1656	−246.1	6.98×10^{-5}
4	−1624	−248.2	7.08×10^{-5}
5	−1632	−241.6	7.24×10^{-5}
6	−1648	−256.7	7.85×10^{-5}
7	−1697	−295.6	1.07×10^{-4}
8	−1640	−234.7	6.11×10^{-5}
9	−1639	−242.4	6.83×10^{-5}
10	−1618	−258.0	6.98×10^{-5}
11	−1623	−259.7	7.54×10^{-5}
12	−1650	−240.2	6.68×10^{-5}
13	−1635	−248.7	6.62×10^{-5}
14	−1583	−259.8	6.62×10^{-5}
15	−1585	−210.1	5.30×10^{-5}

Table 3 Fitting parameters of polarization curves of array electrodes under flow velocity of 3.54 m/s

Electrode No.	φ_{corr} (vs SCE)/ mV	b_c (vs SCE)/ (mV·dec^{-1})	Corrosion current density/(A·cm^{-2})
1	−1528	−231.9	6.42×10^{-5}
2	−1570	−245.5	7.13×10^{-5}
3	−1571	−263.3	7.34×10^{-5}
4	−1590	−250.5	7.75×10^{-5}
5	−1651	−220.3	8.05×10^{-5}
6	−1641	−255.6	9.12×10^{-5}
7	−1655	−262.8	1.11×10^{-4}
8	−1545	−258.7	7.24×10^{-5}
9	−1605	−255.3	8.05×10^{-5}
10	−1559	−246.2	7.34×10^{-5}
11	−1568	−286.7	8.76×10^{-5}
12	−1482	−242.9	7.03×10^{-5}
13	−1575	−253.1	7.34×10^{-5}
14	−1532	−253.6	7.54×10^{-5}
15	−1521	−261.0	7.59×10^{-5}

Table 4 Fitting parameters of polarization curves of array electrodes under flow velocity of 5.31 m/s

Electrode No.	φ_{corr} (vs SCE)/ mV	b_c (vs SCE)/ (mV·dec^{-1})	Corrosion current density/(A·cm^{-2})
1	−1524	−255.7	9.02×10^{-5}
2	−1562	−245.7	8.66×10^{-5}
3	−1551	−259.2	9.17×10^{-5}
4	−1555	−260.8	9.17×10^{-5}
5	−1572	−253.9	9.38×10^{-5}
6	−1607	−258.7	9.94×10^{-5}
7	−1603	−274.4	1.22×10^{-4}
8	−1531	−277.4	9.63×10^{-5}
9	−1521	−281.2	9.78×10^{-5}
10	−1566	−273.6	9.89×10^{-5}
11	−1564	−273.3	9.99×10^{-5}
12	−1543	−265.9	1.00×10^{-4}
13	−1542	−265.9	1.01×10^{-4}
14	−1556	−259.8	1.05×10^{-4}
15	−1537	−278.0	1.15×10^{-4}

3.2 CFD simulation

Figures 6−8 show the three-dimensional distributions of fluid flow velocity and shear stress at the elbow under different flow velocities. Three-dimensional distributions of fluid flow velocity and shear stress along the elbow are symmetrical with respect to the central plane of pipe. Furthermore, the change trends of fluid flow velocity and shear stress at the elbow are the same under different flow velocities, and the shear stress increases with increasing flow velocity. From the

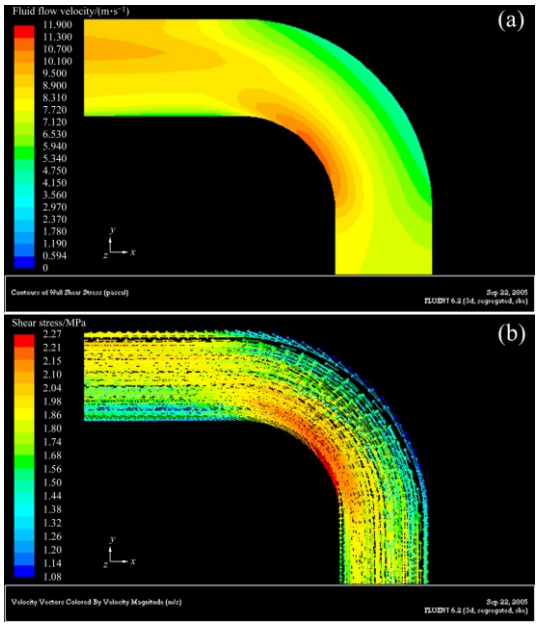

Fig. 6 Three-dimensional distributions of fluid flow velocity (a) and shear stress (b) at elbow under flow velocity of 1.77 m/s

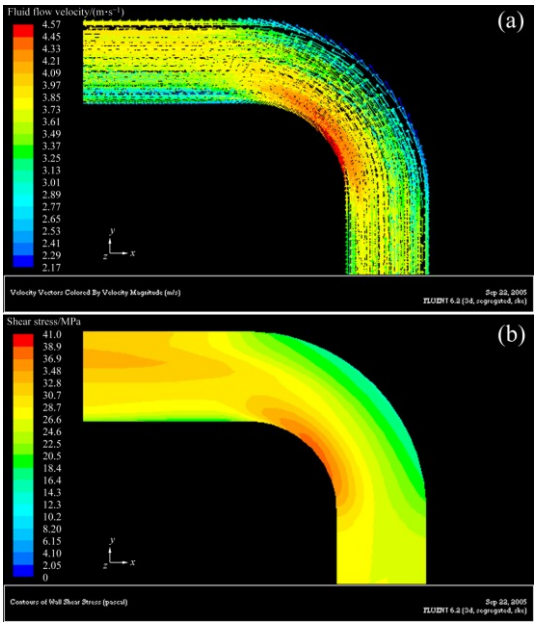

Fig. 7 Three-dimensional distributions of fluid flow velocity (a) and shear stress (b) at elbow under flow velocity of 3.54 m/s

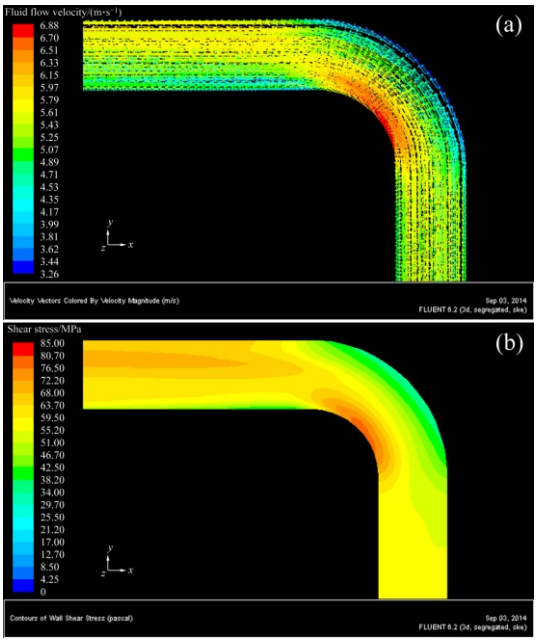

Fig. 8 Three-dimensional distributions of fluid flow velocity (a) and shear stress (b) at elbow under flow velocity of 5.31 m/s

distribution of fluid flow velocity and shear stress at the elbow, flow velocity and shear stress decrease from the innermost side to the outermost side. In the outermost wall of the elbow, flow velocity and shear stress decrease at first, and then increase along the direction of fluid flow. Based on the above analysis, a conclusion can be drawn that the higher flow velocity corresponds to the bigger shear stress, and the lower flow velocity corresponds to the smaller shear stress at the elbow.

3.3 Surface morphology analysis after corrosion test

The surface morphologies of AZ91D magnesium alloy after static state corrosion for 4 h are shown in Fig. 9. It is seen from Fig. 9 that there is a relatively compact and integrated corrosion product film on the electrode surface. Figure 10 shows the surface morphologies of No. 15 AZ91D magnesium alloy electrodes under different flow velocities after corrosion for 4 h. It is seen from Fig. 10 that there are obvious cutting tracks on the surface of these electrodes, which could be attributed to the erosion of fluid on the substrate. Furthermore, the scale of the corrosion product films becomes bigger and bigger with decreasing flow velocity. This can be explained that the removal of corrosion products on the surface of the electrode is easy with the high flow velocity and the large shear stress, but it is difficult for corrosion products to remove with the low flow velocity and the small shear stress. Figures 11−13 show the surface morphologies of representative AZ91D magnesium alloy array electrodes (Nos. 4, 13 and 15 electrodes) under different flow velocities after corrosion for 4 h, respectively. It is seen from Figs. 11−13 that there are obvious cutting tracks on the surface of all these electrodes. When flow velocity is 5.31 m/s, the scale of the corrosion product films becomes more and more greater from the inside to the outside of the elbow. However, when flow velocities are 1.77 and 3.54 m/s, the scale of the corrosion product films is similar from the inside to the outside of the elbow.

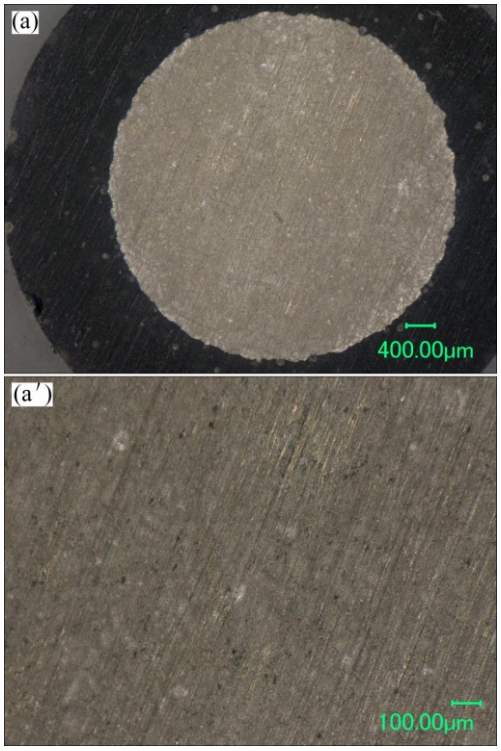

Fig. 9 Surface morphologies of AZ91D after static state corrosion test for 4 h

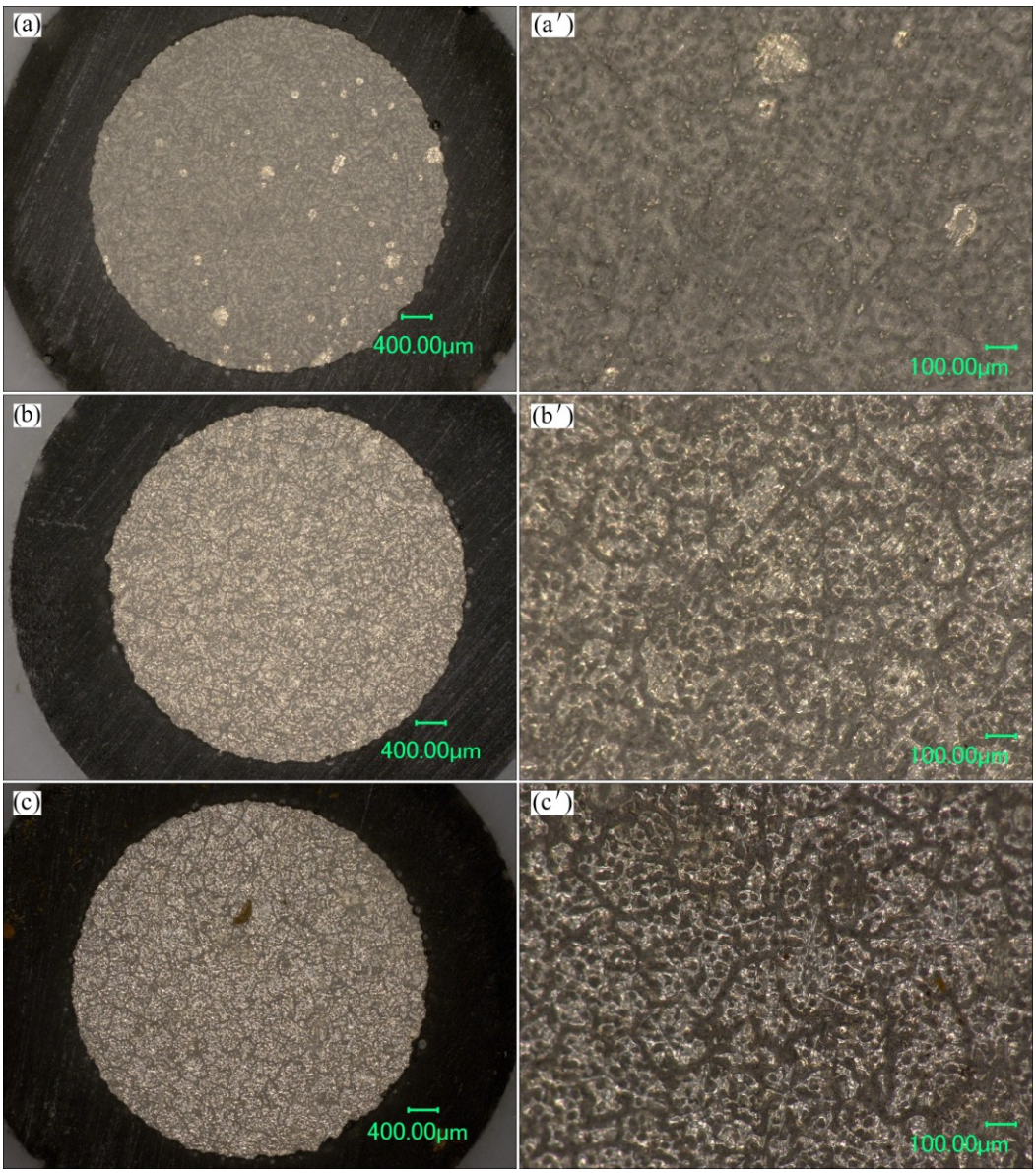

Fig. 10 Surface morphologies of No. 15 electrode under different flow velocities after corrosion test for 4 h: (a, a′) 5.31 m/s; (b, b′) 3.54 m/s; (c, c′) 1.77m/s

4 Discussion

The corrosion of magnesium alloy in containing chloride solution should include anodic dissolution of magnesium and cathodic hydrogen evolution [14], which can always be expressed as reactions (1) and (2):

$$Mg \rightarrow Mg^{+}+e \text{ or } Mg^{+} \rightarrow Mg^{2+}+e \quad (1)$$

$$2H_2O+2e \rightarrow 2OH^{-}+H_2\uparrow \text{ or } 2H^{+}+2e \rightarrow H_2\uparrow \quad (2)$$

Although the corrosion mechanism of magnesium alloys may involve many complicated intermediate steps [8], the overall corrosion reaction can always be expressed as reaction (3):

$$Mg+2H_2O \rightarrow Mg(OH)_2+H_2\uparrow \quad (3)$$

Therefore, a corrosion product film consisting of $Mg(OH)_2$ can be formed on the magnesium alloy surface.

Polarization measurement demonstrates the different electrochemical activities and corrosion behavior for AZ91D magnesium alloy array electrodes under different flow velocities at different locations of the elbow in circulating ASTM D1384−87 solution, as described in Figs. 3−5. According to Figs. 2−5, AZ91D magnesium alloy is in an active dissolution state in the flowing solution, and the corrosion rate of AZ91D magnesium alloy increases with increasing flow velocity, which can be attributed to two reasons, the first is that fluid flow enhances the convection and diffusion of reactive species, accelerating the corrosion electrochemical reactions, and the second is that fluid flow

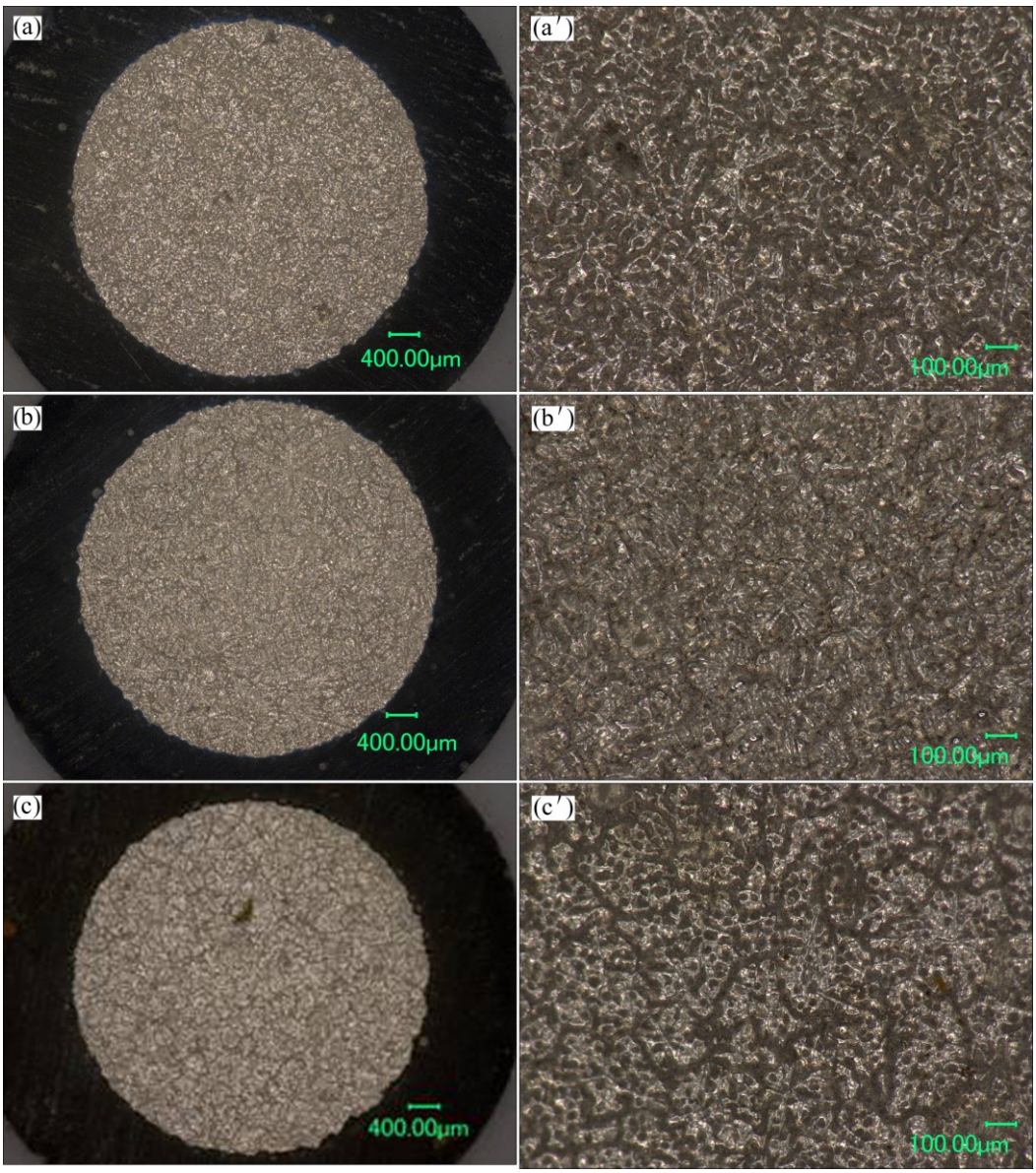

Fig. 11 Surface morphologies of representative electrodes under flow velocity of 1.77 m/s after corrosion test for 4 h: (a, a′) No. 4 electrode; (b, b′) No. 13 electrode; (c, c′) No. 15 electrode

accelerates the removal of corrosion products. When the flow velocity is 5.31 m/s, the distribution of the corrosion rates is in good accordance with the distributions of flow velocity and shear stress at the elbow. However, the distribution of the corrosion rates at the elbow is not in good accordance with the distributions of flow velocity and shear stress at the elbow when the flow velocities are 1.77 and 3.54 m/s, respectively. Furthermore, the distribution of the corrosion rates is exactly opposite with the distributions of fluid flow velocity and shear stress from the inside to the outside of the elbow when the flow velocity is 1.77 m/s. This means that a critical flow velocity could exist in the corrosion of AZ91D magnesium alloy. When the flow velocity is higher than the critical flow velocity, fluid hydrodynamics effects (flow velocity and shear stress) are dominant in the corrosion of AZ91D magnesium alloy. When the flow velocity is lower than the critical flow velocity, electrochemical corrosion factors are dominant in the corrosion of AZ91D magnesium alloy due to the high electrochemical activity of AZ91D magnesium alloy. When the flow velocity is very low, the velocity gradient near the wall is lower, and then $Mg(OH)_2$ formed by electrochemical reactions is easy to deposit on the electrode surface of the surface upward, resulting in a lower corrosion rate.

In this work, the CFD simulation indicates that there are similar distributions of flow velocity and shear stress under different flow velocities at the elbow, while there are quite different flow velocities and shear stress at

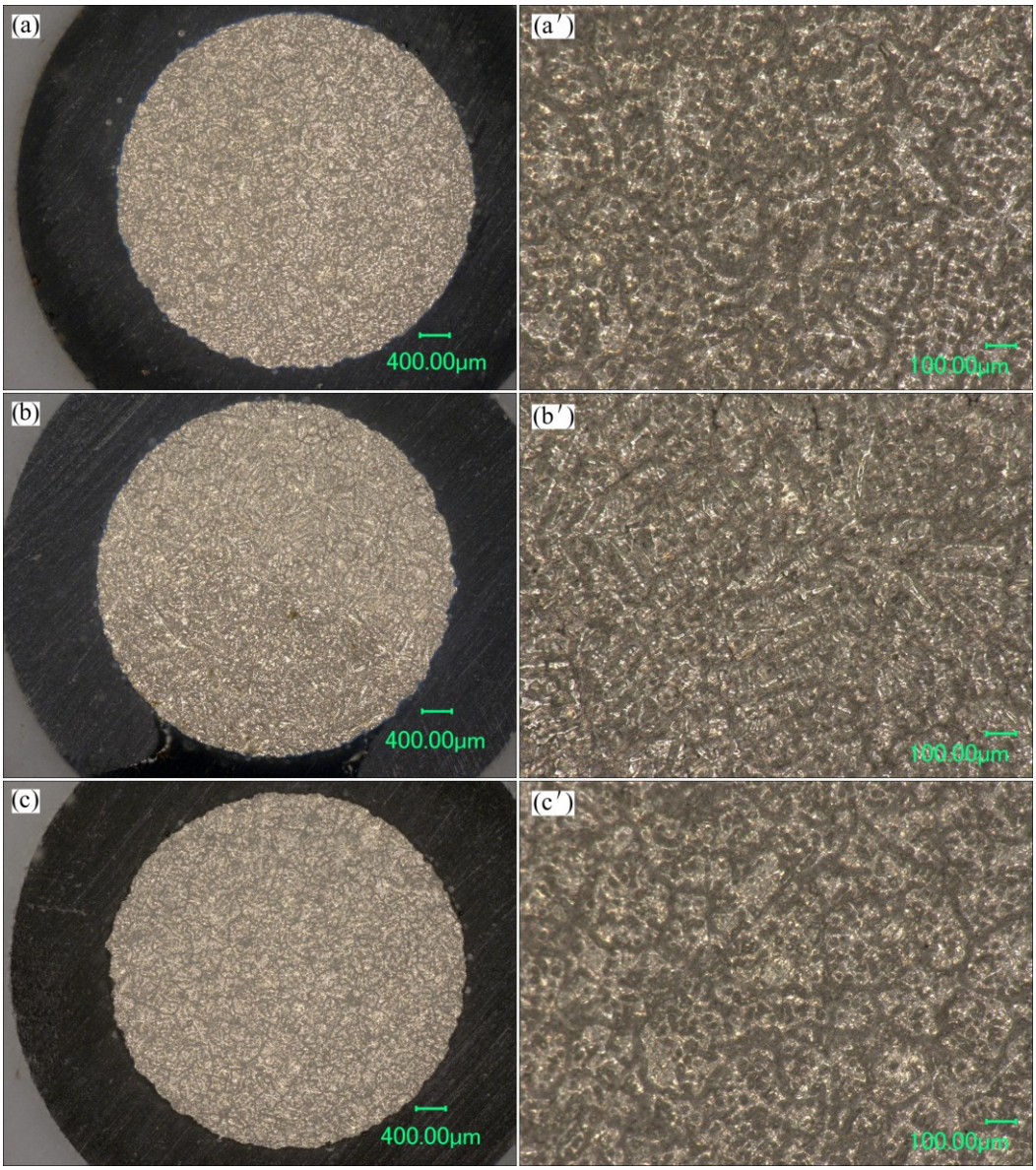

Fig. 12 Surface morphologies of representative electrodes under flow velocity of 3.54 m/s after corrosion test for 4 h: (a, a′) No. 4 electrode; (b, b′) No. 13 electrode; (c, c′) No. 15 electrode

different locations along the elbow under the same flow velocity. By comparing the CFD simulation results with the experimental results, the flow velocity plays a significant role and affects the corrosion of AZ91D magnesium alloy, which may be attributed to that a high flow velocity corresponds to a higher mass transfer rate, accelerating the corrosion electrochemical reactions and the removal of corrosion products on the surface of the electrode, and eventually resulting in increasing corrosion rate. When the flow velocity exceeds the critical flow velocity, the distribution of the corrosion rates is in good accordance with the distributions of flow velocity and shear stress at the elbow, which indicates that fluid hydrodynamics plays a significant role and affects the corrosion of AZ91D magnesium alloy at this time. A higher flow velocity corresponds to a larger shear stress, resulting in a higher corrosion rate. When the flow velocity is lower than the critical flow velocity, the distribution of the corrosion rates is not in accordance with the distributions of fluid flow velocity and shear stress at the elbow, which indicates that electrochemical corrosion factors play a significant role and control the corrosion of AZ91D magnesium alloy at this time. When the flow velocity is 1.77 m/s, the maximum shear stress is only 11.3 Pa (No. 15 electrode). It is difficult to remove the corrosion product film on the electrode surface, and $Mg(OH)_2$ formed by electrochemical reactions is easy to deposit on the electrode surface of the surface upward, so a lower corrosion rate (53 μA/cm^2) is obtained.

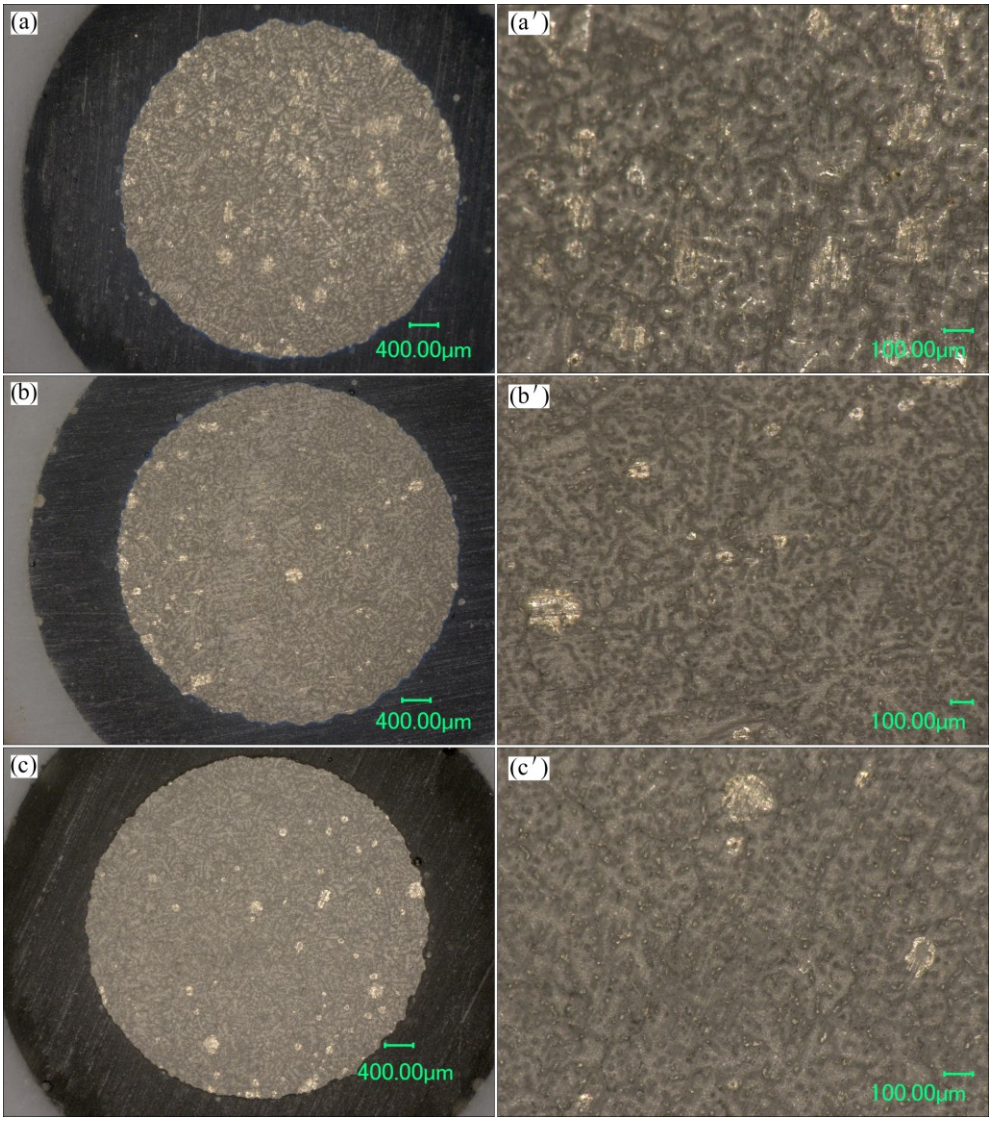

Fig. 13 Surface morphologies of representative electrodes under flow velocity of 5.31 m/s after corrosion test for 4 h: (a, a′) No. 4 electrode; (b, b′) No. 13 electrode; (c, c′) No. 15 electrode

5 Conclusions

1) The corrosion rate of AZ91D magnesium alloy increases with increasing flow velocity, which can be attributed to two reasons, the first is that fluid flow enhances the convection and diffusion of reactive species, accelerating the corrosion electrochemical reactions, and the second is that fluid flow accelerates the removal of corrosion products on the surface electrode.

2) AZ91D magnesium alloy at different locations of the elbow exhibits different corrosion behaviors under different flow velocities.

3) A critical flow velocity could exist in the corrosion of AZ91D magnesium alloy at the elbow. When the flow velocity is higher than the critical flow velocity, fluid hydrodynamics effects (flow velocity and shear stress) are dominant in the corrosion of AZ91D magnesium alloy. On the contrary, electrochemical corrosion factors are dominant in the corrosion of AZ91D magnesium alloy.

References

[1] XU L Y, CHENG Y F. Electrochemical characterization and CFD simulation of flow-assisted corrosion of aluminum alloy in ethylene glycol-water solution [J]. Corrosion Science, 2008, 50: 2094−2100.

[2] XU L Y, CHENG Y F. Effect of fluid hydrodynamics on flow-assisted corrosion of aluminum alloy in ethylene glycol-water solution studied by a microelectrode technique [J]. Corrosion Science, 2009, 51: 2330−2335.

[3] MILLER W S, ZHUANG L, BOTTEMA J, WITTEBROOD A J, de SMET P, HASZLER A, VIEREGGE A. Recent development in aluminium alloys for the automotive industry [J]. Materials Science and Engineering A, 2000, 280: 37−49.

[4] RANJBAR K. Effect of flow induced corrosion and erosion on failure of a tubular heat exchanger [J]. Materials and Design, 2010, 31: 613−619.

[5] SONG G, BOWLES A L, D. ST JOHN H. Corrosion resistance of aged die cast magnesium alloy AZ91D [J]. Materials Science and Engineering A, 2004, 366: 74−86.
[6] ZHANG T, LIU X, SHAO Y, MENG G, WANG F. Electrochemical noise analysis on the pit corrosion susceptibility of Mg−10Gd−2Y−0.5Zr, AZ91D alloy and pure magnesium using stochastic model [J]. Corrosion Science, 2008, 50: 3500−3507.
[7] FEKRY A M, FATAYERJI M Z. Electrochemical corrosion behavior of AZ91D alloy in ethylene glycol [J]. Electrochimca Acta, 2009, 54: 6522−6528.
[8] SONG G, ATRENS A, WU X, ZHANG B. Corrosion behaviour of AZ21, AZ501 and AZ91 in sodium chloride [J]. Corrosion Science, 1998, 40: 1769−1791.
[9] SEIFZADEH D, BEZAATPOUR A, ASADPOUR JOGHANI R. Corrosion inhibition effect of N, N′-bis (2-pyridylmethylidene)-1,2-diiminoethane on AZ91D magnesium alloy in acidic media [J]. Transactions of Nonferrous Metals Society of China, 2014, 24(11): 3441−3451.
[10] GUO H, MA Y, WANG J, WANG Y, DONG H, HAO Y. Corrosion behavior of micro-arc oxidation coating on AZ91D magnesium alloy in NaCl solutions with different concentrations [J]. Transactions of Nonferrous Metals Society of China, 2012, 22(7): 1786−1793.
[11] TIAN Y, YANG L, LI Y, WEI Y, HOU L, LI Y, MURAKAMI R. Corrosion behaviour of die-cast AZ91D magnesium alloys in sodium sulphate solutions with different pH values [J]. Transactions of Nonferrous Metals Society of China, 2011, 21(4): 912−920.
[12] ZHOU W, SHEN T, AUNG N. Effect of heat treatment on corrosion behaviour of magnesium alloy AZ91D in simulated body fluid [J]. Corrosion Science, 2010, 52: 1035−1042.
[13] ARRABAL R, PARDO A, MERINO M C, MOHEDANO M, CASAJÚS P, PAUCAR K, GARCÈS G. Effect of Nd on the corrosion behaviour of AM50 and AZ91D magnesium alloys in 3.5 wt.% NaCl solution [J]. Corrosion Science, 2012, 55: 301−312.
[14] SONG G L, LIU M. Effect of Nd on the corrosion behaviour of AM50 and AZ91D magnesium alloys in 3.5 wt.% NaCl solution [J]. Corrosion Science, 2012, 62: 61−72.
[15] ZHANG G A, ZENG L, HUANG H L, GUO X P. A study of flow accelerated corrosion at elbow of carbon steel pipeline by array electrode and computational fluid dynamics simulation [J]. Corrosion Science, 2013, 77: 334−341.
[16] LEE S, KIM S. Microstructure and mechanical properties of TiN/TiAlN multilayer coatings deposited by arc ion plating with separate targets [J]. Transactions of Nonferrous Metals Society of China, 2011, 21: 1703−1709.
[17] WHARTON J A, WOOD R J K. Erosion-corrosion resistance of engineering materials in various test conditions [J]. Wear, 2004, 256: 525−536.
[18] LU B T, LUO J L, GUO H X, MAO L C. Erosion-enhanced corrosion of carbon steel at passive state [J]. Corrosion Science, 2011, 53: 432−440.
[19] RAJAHRAMN S S, HARVEY T J, WOOD R J K. Electrochemical investigation of erosion-corrosion using a slurry pot erosion tester [J]. Tribology International, 2011, 44: 232−240.
[20] JIAND X, ZHENG Y G, KE W. Effect of flow velocity and entrained sand on inhibition performances of two inhibitors for CO_2 corrosion of N80 steel in 3% NaCl solution [J]. Corrosion Science, 2005, 47: 2636−2658.
[21] LOPEZ D, FALLEIROS N A, TSCHIPTSCHIN A P. Effect of nitrogen on the corrosion-erosion synergism in an austenitic stainless steel [J]. Tribology International, 2011, 44: 610−616.
[22] MOHAMMADI F, LUO J, LU B, AFACAN A. Single particle impingement current transients for prediction of erosion-enhanced corrosion on 304 stainless steel [J]. Corrosion Science, 2010, 52: 2331−2140.
[23] STACK M M, ABDULRAHMAN G H. Mapping erosion-corrosion of carbon steel in oil exploration conditions: Some new approaches to characterizing mechanisms and synergies [J]. Tribology International, 2010, 43: 1268−1277.
[24] MALKA R, NESIC S, GULINO D A. Erosion-corrosion and synergistic effects in disturbed liquid-particle flow [J]. Wear, 2007, 262: 791−799.
[25] RIHAN R O, NESIC S. Erosion-corrosion of mild steel in hot caustic. Part I: NaOH solution [J]. Corrosion Science, 2006, 48: 2633−2659.
[26] EL-GAMMAL M, MAZHAR H, COTTON J S. The hydrodynamic effects of single-phase flow on flow accelerated corrosion in a 90-degree elbow [J]. Nuclear Engineering and Design, 2010, 240: 1589−1598.
[27] HU J, HUANG D, SONG G, GUO X. The synergistic inhibition effect of organic silicate and inorganic Zn salt on corrosion of Mg-10Gd-3Y magnesium alloy [J]. Corrosion Science, 2011, 53: 4093−4101.

弯管段流速对 AZ91D 镁合金腐蚀行为的影响

田 径[1]，黄华良[1,2]，潘志权[1]，周 红[1]

1. 武汉工程大学 化学与环境工程学院，武汉 430073；
2. 华中科技大学 化学与化工学院，武汉 430074

摘 要：基于阵列电极技术使用自制的环路系统并采用极化、计算流体力学(CFD)模拟和表面分析技术研究环路系统中弯管段流速对 AZ91D 镁合金腐蚀行为的影响。实验结果表明，AZ91D 镁合金的腐蚀速率随着流速的增加而增加，且 AZ91D 镁合金在流动介质中的腐蚀可能存在临界流速。当介质的流速超过临界流速时，流体力学因素在 AZ91D 镁合金腐蚀中占主导地位；反之，电化学腐蚀因素占主导地位。

关键词：镁合金；流速；弯管；计算流体力学(CFD)；极化

(Edited by Xiang-qun LI)